Research Article

Cheah Chee Ban*, Mohammed A. Khalaf, Mahyuddin Ramli, Naser M. Ahmed, Bassam M. Abunahel, Eethar Thanon Dawood, and Farshad Ameri

Effect of nano-silica slurry on engineering, X-ray, and γ-ray attenuation characteristics of steel slag high-strength heavyweight concrete

https://doi.org/10.1515/ntrev-2020-0098
received October 18, 2020; accepted November 28, 2020

Abstract: High molar mass materials (nano-silica slurry [NSS] and aggregate of steel furnace slag [ASFS]) can improve concrete shielding properties. However, only a few studies have been reported in this regard. Hence, this paper aims to determine the effect of NSS and ASFS on the properties of the resulting steel slag heavyweight concrete (SSHWC). The use of NSS in this study is a novel contribution. Furthermore, the maximum percentage of NSS to be introduced into the concrete for maximum effect was also optimized. This study also implemented an investigation program with six concrete mixtures prepared using ASFS as the primary by-product aggregate. The engineering, X-ray, and γ-ray attenuation characteristics of the SSHWC were evaluated. The results showed that the addition of NSS in SSHWC at the optimal content of 3% by weight of cement improved the X-ray shielding by 6.4%. Besides, all the concrete's engineering and γ-rays' properties were enhanced correspondingly.

Keywords: X-ray, nano-silica slurry, shielding concrete, heavyweight aggregate, gamma-ray

List of abbreviations

ASFS	aggregate of steel furnace slag
ASTM	American Society of Testing Materials
BS	British Standard Institute
CS	compressive strength
FE-SEM	field emission scanning electron microscope
HVL	half-value layer
HWC	heavyweight concrete
ITZ	internal transition zone
MS	Malaysia standard
NSS	nano-silica slurry
OPC	ordinary Portland cement
SEM	scanning electron microscope
SSHWC	steel slag heavyweight concrete
STS	splitting tensile strength
TEM	transmission electron microscopy
TVL	tenth value layer
UHPCs	ultra-high performance concrete
UPV	ultra pulse velocity
W/C	water to cement ratio
XRD	X-ray diffraction
ZPV	zeta potential value
γ-ray	Gamma-ray
μ	linear attenuation coefficient

1 Introduction

Lasting buildings are specifically aimed at reducing the harmful environmental impact of the building industry. The rapid rate of industrialization has contributed to the rapid rate of waste generation, which makes waste management a global problem with a detrimental effect on the climate. The construction industry sector contributes significantly to the waste management in the construction industry, as this sector produces large amounts of waste materials in building activities [1]. Nonetheless, the

* **Corresponding author: Cheah Chee Ban,** School of Housing, Building and Planning, Universiti Sains Malaysia, 11800 USM, Gelugor, Malaysia, e-mail: cheacheeban@usm.my
Mohammed A. Khalaf, Mahyuddin Ramli, Farshad Ameri: School of Housing, Building and Planning, Universiti Sains Malaysia, 11800 USM, Gelugor, Malaysia
Naser M. Ahmed, Bassam M. Abunahel: School of Physics, Universiti Sains Malaysia, 11800 USM, Gelugor, Malaysia
Eethar Thanon Dawood: Building and Construction Engineering Department, Technical Engineering College of Mosul, Northern Technical University, Mosul, Iraq

metallurgical waste from the manufacturing processes of steel and iron has great concern regarding its management. For instance, blast furnace slag is a by-product formed during pig iron production [2]. This waste is usually processed and used as a raw material in other manufacturing processes. Even so, most of the metallurgical wastes are deposited in landfills as they are generated in huge quantities [3]. Owing to the environmental effect of these wastes when deposited in landfills, it has become a necessity to minimize the quantity of steel and iron wastes generated from production activities by exploring novel ways of using the wastes for economic benefits. The slag is produced as waste material from iron and steel manufacturing processes, and it can be used as a raw material in other sectors [4–6]. It contributes to the management of slag impacts on the environment. The aggregate of steel furnace slag (ASFS) is a waste material of the steel processing industry that formed during the smelting of pig iron and scrap metal in the electric arc furnaces [7].

The previous study focused on putting forward some of the production percentages of ASFS for different countries, in which utilization rate of ASFS is low. India generates 72.2 million metric tons of steel every year and produces almost 1,80,00,000 MT of waste; however, only about 25% of the quantity produced is used in cement production. The output of the European Union is at 10 million per year, of which 1.5 million per year is attributed to Spain [8]. Heavyweight concrete (HWC) is a specific concrete type primarily used as a nuclear reactor shielding wall [9]. Concrete materials that contain aggregates of heavy elements show strong radiation protective properties, as the incorporation of these aggregates in HWC enhances the neutron and proton absorption ability of HWC [10,11]. Khalaf et al. carried out a comprehensive study of HWC [12] and found that concrete with >2,600 kg/m^3 density is classified as HWC. Other studies stipulate that concrete must have a density of at least 3,000 kg/m^3 to be considered HWC [8,13]. Normally, HWC serves as embodiments in structures that barricade the emission of a high dose of radioactive rays to avoid harmful effects on people. Therefore, HWC is mainly used in nuclear reactor sites and other structures like hospitals, radiotherapy systems, and facilities for the storage of radioactive wastes [14]. Because of these critical HWC functions and characteristics, it is necessary for these concretes to be dense and designed to the desired purpose. Therefore, the heavyweight aggregates must be used for the manufacture of concrete to meet these purposes [15,16].

Previous researchers [17,18] have agreed on the necessity of testing the behavior of concrete in isolating harmful radiation (such as X-rays) to humans. The need to identify the characteristics of concrete for the isolation of X-rays arises for various industrial applications such as the production of devices and laboratories with exposure to a high dose of X-ray radiations. A significant trend in modern structural engineering is the production of a more robust and sustainable concrete to reduce the life-cycle costs of structures. Nanotechnology has opened up a new world in the field of building and construction materials [19,20]. The fineness increment of the material widens its applications in various applications, such as in structural, automotive, marine, and military [21,22], as the nanostructures are playing significant roles in the development of new functions and the enhancement of the existing functions of industrial applications, because of their piezoelectricity, biocompatibility, and pyroelectrical characteristics. The work focused on the review of the characteristics, applications, working mechanism and production method of different nanomaterials [22]. Many nanomaterials have been examined for use in the construction sector, such as nano-silica, nano-clay, $CaCO_3$ nanoparticles, nano-titania, carbon nanotubes, graphene oxide, and nano-alumina [23,24]. To study the effect of nano-graphene on chloride penetration resistance of recycled concrete, ultra-high-strength nano-graphene oxide with good hydrophilicity and dispersibility was used to investigate the mechanism of action. The results showed that nanomaterials fill the recycled concrete micro-cracks, decrease the most probable aperture, increase the number of harmless small apertures, and improve the volume stability of recycled concrete, thereby improving the resistance to chloride penetration, which is important for improving concrete durability [24].

The application of nano-silica has led to substantial improvements in the mechanical properties of cementitious materials [25]. Zhuang and Chen [26] have also reported that the improvement effect of nano-SiO_2 on concrete is remarkable, especially in the aspect of enhancing the durability of concrete. Recent studies suggested that nanotechnology can help in achieving significant technological advancement, particularly in the field of producing alternative cementitious materials. Hence, nanotechnology can be used significantly in improving mix designs, manufacturing processes, and workability of cement-based materials [27]. Nano-silica exists in two forms: dry grain densified and colloidal suspension. A unique method is needed for drying nano-silica before mixing so that the nanoparticles become distributed uniformly within the solvent [28–30].

In a recent study on the use and production of circular nano-silica concrete-filled stainless steel tube, the

study provides for testing the resulting concrete for environmental factors as in a number of the freeze-thaw cycle test. The study was expanded to include design calculations for the bearing capacity of nano-silica concrete-filled stainless steel tub column. The result of the study showed that the extent of the improved ability of nanomaterials was optimistic and could be expanded to include different applications [30]. Contrarily, colloidal nano-silica is developed as a stabilized suspension using a dispersive agent [31]. A related study [32] proposed that colloidal nano-silica application to mortar mixes enhanced the mixing uniformity. It was attributed to improved dispersion behavior and low nano-silica agglomeration rate in the mixture, which facilitated the distribution.

The characteristics of the pozzolanic reactivity of nano-silica were investigated to understand its pozzolanic reaction kinetics, the morphology of hydrates structure, and effect on the properties of cement-based materials [33]. Land and Stephan [34] studied the effect of various nanoparticles on the cement hydration. The cement hydration acceleration depended on the total surface area of the nano-silica particles. The inclusion influence of colloidal nano-silica on microstructure and hardened properties of ultra-fine cement have been investigated. The ideal content of nano-silica was found to be 4% by weight of cement [35]. The filler effect was responsible for decreased pore volume, finer pore size distribution, and improved physicomechanical characteristics of the mortar. However, because of agglomeration, the addition of powders in amounts exceeding 1.25% increased the pore volume of certain mortars [36].

The nano-silica is similar to the silica fume, which improves the paste and concrete packing density, especially at the internal transition zone (ITZ) between pastes and aggregates. At 90 days, 1% of nano-silica affects approximately equal to or similar to that of 10% of micro-silica. On the contrary, with nano-silica above 2% (e.g., 3% by weight of cement), the resulting performance of concrete was still higher than those without nano-silica (control concrete mix). The binary use of nano and micro-silica was found to have a better impact on the characteristics of ultra-high performance concrete (UHPCs) compared to their impacts [37]. Because of the high reactivity of nanoparticles and fillers, they can serve as nuclei for cement phases, which encourage cement hydration that enhances the micro-structure density and reduces the porosity of the ITZ. Results showed that the density and mechanical properties in the ITZ were obviously improved by nano-strengthening.

The penetration of nanomaterials was helpful to block the pores and cracks in the ITZ, as well as to avoid the directed gathering of CH crystal. The most significant problem for all nanoparticles is effective dispersion. The use of nanoparticles at high dosage impaired the advantages of their small individual particle size and produced unreacted clusters of agglomerated particles. It may lead to an increased potential for stress concentration in the material. The nano-silica was reported to improve the strength and workability of concrete, as well as to improve water permeation resistance. Furthermore, the large and reactive nature of nanoparticles coating has been shown to accelerate hydration reactions of C3S phase in cement mortar [38].

In another study, the nano-silica was applied in five percentages (1%, 2%, 3%, 4%, and 5%) by weight of cement. The results showed 3% nano-silica content from cement weight as the optimum [39]. Nano-silica addition was reported to achieve better mechanical performance, and the study attempted to investigate the effect of various parameters on the axial compressive behavior of nano-silica concrete-filled angle steel-reinforced GFRP tubular columns. It was found that as the nano-silica concrete compressive strength (CS) of the specimens increased, the load-bearing capacity and initial stiffness increased. However, specimens with a higher CS of nano-silica concrete showed lower deformation capacity than specimens with a lower CS of nano-silica concrete [40]. However, the excessive dosage or dispersion of nano-silica will affect the concrete mechanical properties in an inverse manner [41]. It has gained much research attention since the discovery of nanomaterials regarding the effect of nanomaterials on properties of concrete.

Various nano-additives were found to perform better compared to other micro counterparts. For instance, it was found that there is a two-fold increase in the early age CS in concrete that produced with nano-silica (size = 40 nm) as compared with the silica fume concrete mix (0.10 μm) [42]. The findings showed that the UHPC's CS increased with the increase in nano-silica content up to 3%, and the mechanical characteristics dropped slightly because of nano-silica agglomerations when the nano-silica contents are above 3%. The addition of nano-silica accelerated the hydration process of cement. The increase in nano-silica content resulted in decreasing the porosity and the average diameter of the pore. For nano-silica specimens, the microstructure was more homogeneous and compact compared to the control specimen [43].

A recent study by ref. [44] reviewed the importance of using nanomaterials, such as nano-silica, nano-calcium carbonate, and nano-zinc oxide, to improve the characteristics of HWC. Researchers have reported the use of nano-titanium [45,46] and nano-ferrite [47] for this purpose. The results showed the positive effects of nanomaterials on the improvement of all HWC-related properties. Therefore, it is desirable to use nanomaterials as additives in HWC. Hence, this study aims to evaluate the suitability of adding nano-silica slurry (NSS) to enhance the (X-ray and γ-ray) engineering attenuation properties of HWC using ASFS.

2 Experimental program

2.1 Materials

2.1.1 Cement, superplasticizer, and ASFS

In this study, the ordinary Portland cement (OPC) 42.5 N used as a binder met BS EN 197-1 criteria [48] as CEM I. The cement was mixed with a superplasticizer compliant with ASTM C494 to achieve efficient dispersion [49]. The polycarboxylate ether superplasticizer used was procured commercially as WP 30. It was used to ensure the fresh concrete that meets the desired workability at low w/c ratios. ASFS was used as aggregate, which is a waste product that is readily available in Malaysia. It is used as both fine and coarse aggregates in concretes. The chemical and physical properties of the ASFS used in this work have been previously reported by ref. [8].

2.1.2 Nano-silica slurry

MC-Bauchemie provided the NSS used in this study. The material was made from undensified nano-silica to ensure full dispersion. The suspension has a relative density of 1.38 g/cm^3. The FE-SEM micrographs for NSS are shown in Figure 1(a) after 24 h of drying in an oven. The TEM images of NSS are shown in a liquid state in Figure 1(b). They confirm that the physical characteristics of the suspended particles are identical to those of the dried form. The results of the FE-SEM and TEM showed a particle size range of 60–100 nm [13]. The NSS XRD pattern is shown in Figure 2. The NSS consisted of silicon carbide in the mineral phase. The chemical composition of the NSS is presented in Table 1.

2.2 Mix design

The steel slag heavyweight concrete (SSHWC) was produced with ASFS (fine and coarse) to evaluate the impact of NSS on the engineering, gamma-ray, and X-ray protective properties of the concrete. The mix design was carried out using the approved procedures in ACI 211.1R. This study adopted the absolute volume mix design technique because it is the standard way of proportioning HWC material [8]. In terms of nomenclature, the mix S1.0 represents concrete mix containing 1.0% NSS as cement additive. The mix designs of the study are presented in Table 2.

The cement contents (fine and coarse) ASFS were fixed at a ratio of 1:2:3 [8]. The NSS was used to increase the percentage of C–S–H and to serve as a filler in the ITZ. In addition, the incorporation of the nanomaterial was aimed at increasing the atomic number of SSHWC. For the composite materials, the effective atomic number (Z_{eff}) is the average number of electrons in the materials that actively take part in the interaction [50]. The aggregate was used in the saturated dry surface condition to prevent the effect of water absorption during the mixing process. A fixed w/c ratio of 0.23 was used for all the mixes while adjusting the superplasticizer content to achieve 100–120 mm constant fresh concrete slump.

2.3 Mixing samples

The samples were mixed as normal concrete in the following manner. First, the ASFS (fine and coarse) was added to the mixer, followed by 2 min dry-mixing with cement. Then, the mixture was homogenized with water, followed by adding about 80% from the required mixing water volume and further mixing for 90 min. Finally, the remaining 20% of the amount of water needed was added gradually. The whole mixing time was 5 min for all the batches to prevent the segregation of aggregates [13]. After mixing, the resulting concrete was subjected to a slump test recommended by ASTM C143 for workability assessment [51].

3 Methods of treatment and tests

3.1 X-ray attenuation measurement

The mass attenuation coefficient of the concretes was measured in the X-ray fluorescence instrument. The high purity

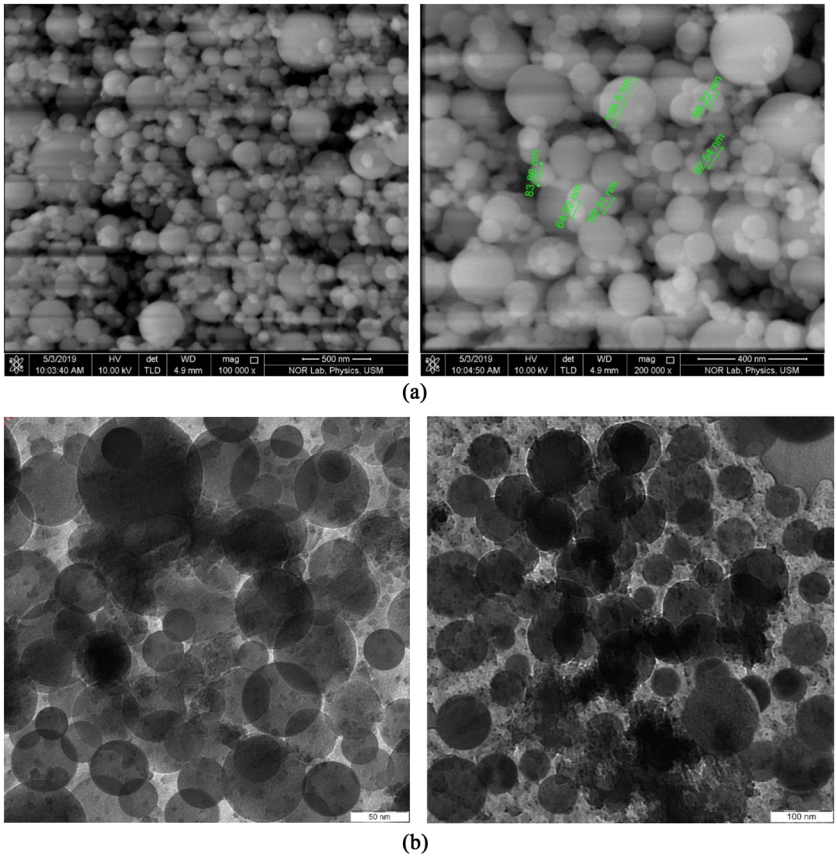

Figure 1: (a) FE-SEM and (b) TEM images of the NSS, adapted from ref. [13].

metal plate (Tungsten; see Figure 3) was irradiated with a 59.54 keV (peak) of 100 mCi 241 Am to produce the characteristic X-ray with 59.32 keV kα energy as shown in Figure 4. The X-ray photons were attenuated by the absorber and detected by CANBERRA low energy Germanium (LEGe) detector with narrow beam geometry. The ORTEC 572 amplifier amplified the detector output pulses, and the spectrum was collected by a multichannel analyzer (MCA-3 series) for

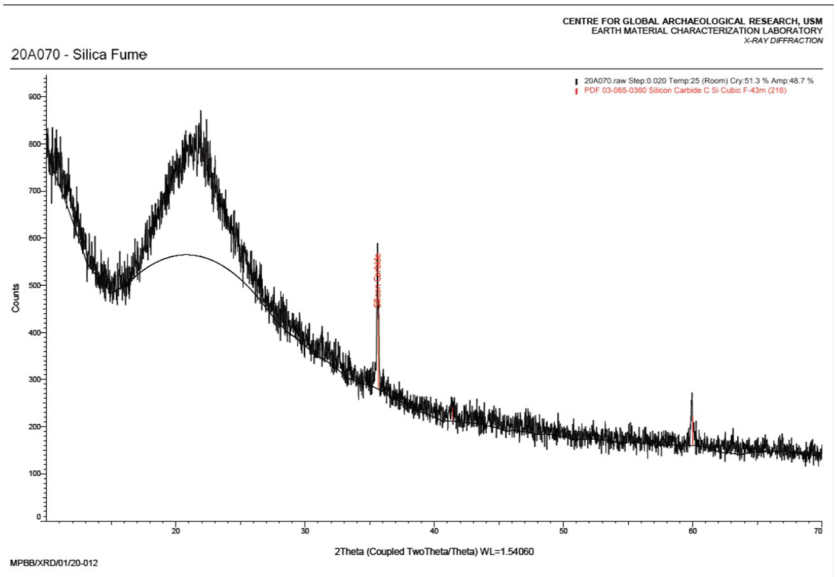

Figure 2: Mineralogy of NSS, adapted from ref. [13].

Table 1: The chemical composition of NSS (wt%)

Oxides	NSS
SiO_2	95.77
TiO_2	0.01
Al_2O_3	0.61
Fe_2O_3 (*t*)	0.11
MgO	0.35
CaO	0.27
Na_2O	0.06
K_2O	0.32
P_2O_5	0.04
Total	97.53

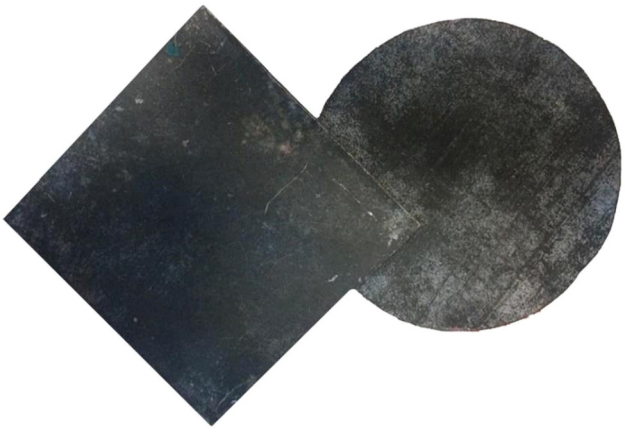

Figure 3: Tungsten used in the study.

10 min. The 20 mm thick test concrete samples were positioned, as shown in Figure 4. The average reading of the three samples was taken for each mix. Each sample was analyzed for 10 min at 7, 28, and 90 days of sample ages. The calculation of the test results was done using the same previous attenuation measurement of γ-ray [8,52].

3.2 The γ-ray attenuation measurement

The attenuation properties of concretes for γ-ray were evaluated by calculating the linear attenuation coefficient (μ), tenth value layer (TVL), and half-value layer (HVL), as previously done in the study by ref. [8]. The experimental setup and stand device used for the γ-rays test in this study are shown in Figure 5. The 100 mm thick test samples were positioned between the γ-ray source and the detector. An average of three samples per mix was used for this test at 7, 28, and 90 days of age.

3.3 Zeta-potential measurement

The nanomaterial was assessed for zeta-potential distribution. One milliliter of each sample was dispersed in 10 mL of distilled water; 5 mL of this solution was placed in a cuvette and investigated for particle stability on a dynamic light scattering equipment. The outcome of this assessment was taken as the zeta potential of the sample.

3.4 Physical and mechanical properties of SSHWC

Different tests were aimed at the physicomechanical properties of the produced SSHWC. The first test on the concrete samples was the slump test, as prescribed in BS EN 26-1-2 [53], which aimed at determining the workability of the fresh concrete. The slump level was classified as S3 in MS EN206, where it was controlled within 100–120 mm. The slump level was classified as S3 in BS EN 206, which was controlled within 100–120 mm [54]. After the mixing process, a density test on the fresh concrete was also carried out. For each batch of concrete, an average of three samples was tested. Then, the next test was the bulk density test of hardened concrete, which was done according to the BS EN 12390-7:2009 specification [55]. The samples were treated for 2, 7, 14, 28, 56 and 90 days, taking into consideration an average density of three samples.

Table 2: SSHWC mixing ratios/1 m^3

Mixes	Cement (kg/m^3)	Fine ASFS (kg/m^3)	Coarse ASFS (kg/m^3)	Nano-silica (%)	w/b ratio (%)	Superplasticizer (%)	Slump (mm)
S0.0	486	972	1,458	0.0	0.23	1.2	110
S1.0	486	972	1,458	1.0	0.23	1.2	118
S2.0	486	972	1,458	2.0	0.23	1.1	110
S3.0	486	972	1,458	3.0	0.23	1.1	115
S4.0	486	972	1,458	4.0	0.23	1.0	110
S5.0	486	972	1,458	5.0	0.23	1.0	105

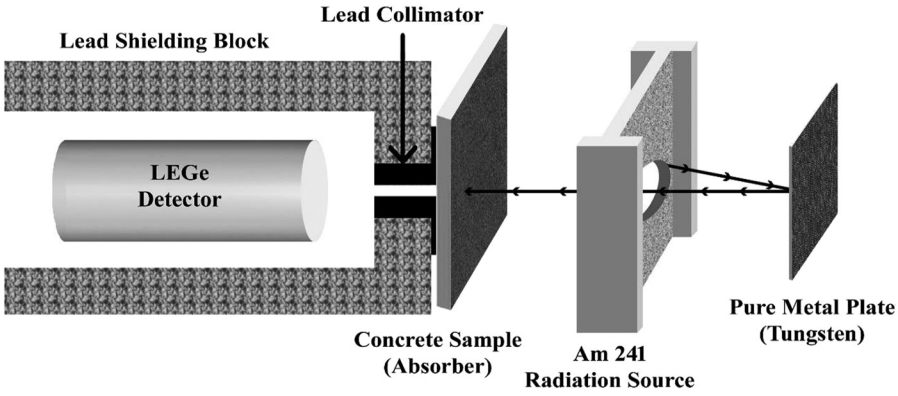

Figure 4: Schematic of the narrow-beam geometry experiment (X-ray experiment).

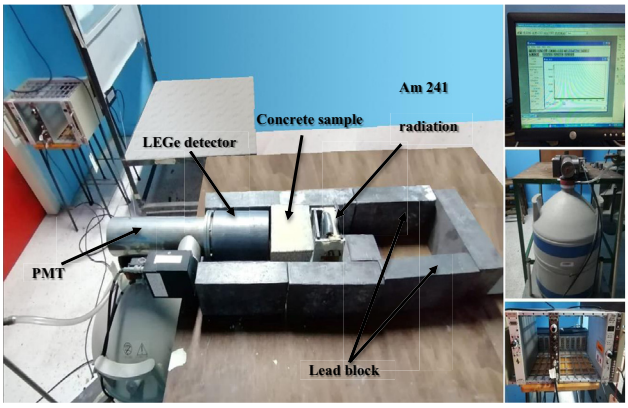

Figure 5: The test stand of γ rays, adapted from ref. [8].

The CS was established for 2, 7, 14, 28, 56, and 90 days after treatment, according to the BS EN 12390-3 recommendation [56]. The CS test was done on the samples after 30 min of removal from the water tank. In addition, the UPV test was performed on the samples according to the BS EN12504-4 specification [57]. Before the CS test, the pulse velocity of the test samples was noted at different sample ages. Splitting tensile strength test was also performed on the sample cylinders of height = 100 mm and diameter = 200 mm. After treating the concrete cylinders 7, 28, and 90 days, the test was performed according to the ASTM C496-96 specification [58].

3.5 Sorption properties measurement and characteristics of microstructural appraisal

The samples were tested for water absorption according to the BS 1881-122 specification [59]. Three sample cylinders of 75 mm diameter and 100 mm height were prepared for the test. They are tested at 2, 7, 14, 28, 56, and 90 days of age.

The capillary absorption test was performed as recommended by ref. [60] to determine the relative sample pore size distribution. The outcome of the test was reported as the coefficient of capillary absorption ($C_{a(t)}$) at (g/cm^2). Three sample prisms of 40 × 40 × 160 mm were prepared and treated for 7 days before the test.

A scanning electron microscopy (SEM) was done to assess the quality of paste's microstructure of the concrete. The results were used to explain the mechanical and pore structure properties of the concrete. The SEM of the hardened samples was tested for the microstructural evolution of concrete composites for the prepared mixes at 28 days of age [8].

4 Results and discussion

4.1 Zeta potential

The surface charge of nanoparticles is an essential property, which shows the stability of the material in suspension, as well as its uniform dispersion in water devoid of agglomeration. It is important that nanomaterials show uniform dispersion when combined with other concrete components. In the concrete mix, the uniform distribution of nanomaterial improves the radiation attenuation property, and it can cover the cement particles, thereby increasing its radiation attenuation properties [61].

The surface zeta potential values (ZPVs) of NSS are given in Figure 6, which showed good ZPVs of the NSS (−29.5 mV). This value indicates that the NSS has a low

potential to agglomerate. A negative ZPV means a negative organic molecule covering the metal nanoparticles; therefore, the stability is increased in suspension during the regarding of aggregation [13]. Nanoparticles that show surface ZPV of −30 mV to +30 mV are considered stable with low potential for agglomerating. The result is considered to be good within these limits, whereas it is an excellent result at >±30 mV. For medical applications, such results are necessary, as it takes longer stability time than using as a constituent concrete material [62].

4.2 The SSHWC workability

The concrete workability refers to the ease of compacting and finishing fresh concrete. The slump test is commonly used to determine concrete workability. The slump values of all the concrete mixes were within 100–120 mm. The amount of cement used for all mixes is relatively high (486 kg/m^3). Therefore, the minimum superplasticizer utilization is 1%; this could be attributed to the large surface area of the cement particles [63]. The amount of superplasticizer was about 1% lower for the S5.0 mix compared to 1.2% of mix S0.0, as presented in Table 2. The spherical shape of the nano-silica particles (as shown in Figure 1) provided a "ball bearing" effect that improved the workability of the fresh concrete. The positioning of HWC at the lowest slump level is commonly recommended. The specific factors to be considered during the designing of HWC mixes for use in construction works are the pumping requirements, the formwork specifics, the placement conditions, and the reinforcement spacing [44].

4.3 The fresh and hardened density of the SSHWC

The fresh SSHWC displayed values of density ranging between 3,000 and 3,004 kg/m^3. The addition of NSS increases the density of concrete because the material that fills the voids and the interface at the ITZ is improved correspondingly. The control mix (S0.0) is the strongest combination of many mixtures that were tested in any earlier studies [8]. In this study, a fixed concrete mixing proportion was maintained for all mixes (1:2:3) (see Table 2).

However, as summarized in Figure 7, it is important to have differences in hardened concrete densities, especially at an early age. Such difference normally comes from the addition of relatively small amounts of nanomaterials relative to the total concrete weight. However, the concrete showed increased hardened densities because of the role of NSS, which facilitated the primary cement hydration by interacting with the cement at the nucleation sites. At the early concrete age, the C–S–H gel was further produced in the matrix of a produced concrete binder. An improved bonding was observed between the aggregates and cement paste, as the nanoparticles occupy the voids in the ITZ [64].

The increase in NSS content up to 3% would improve the density of the concrete at an early age; it is essential for better protection from radiation. Besides, the higher NSS content of 4% resulted in negative effects, as depicted in Figure 7. It could be caused by the difficulty in homogenizing the NSS at higher contents. It could also be attributed to the larger amount of water contained in NSS, which makes the real w/c ratio higher. The presence of entrapped air reduced the rheological property; it also affected the density of the concrete [13]. The mechanical

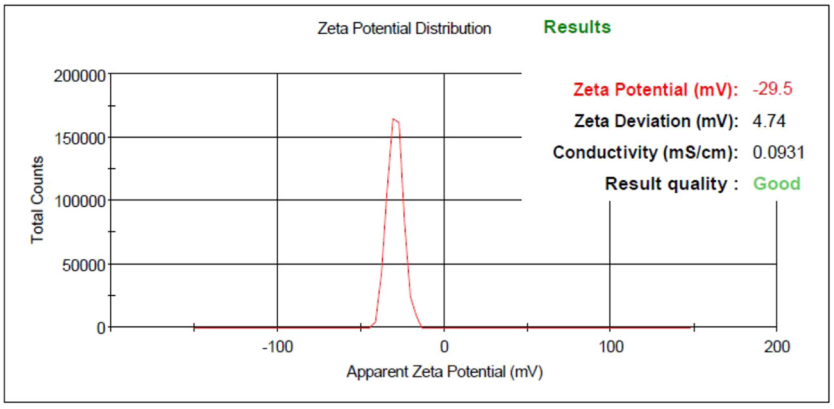

Figure 6: Surface charge (zeta potential) value of NSS, adapted from ref. [13].

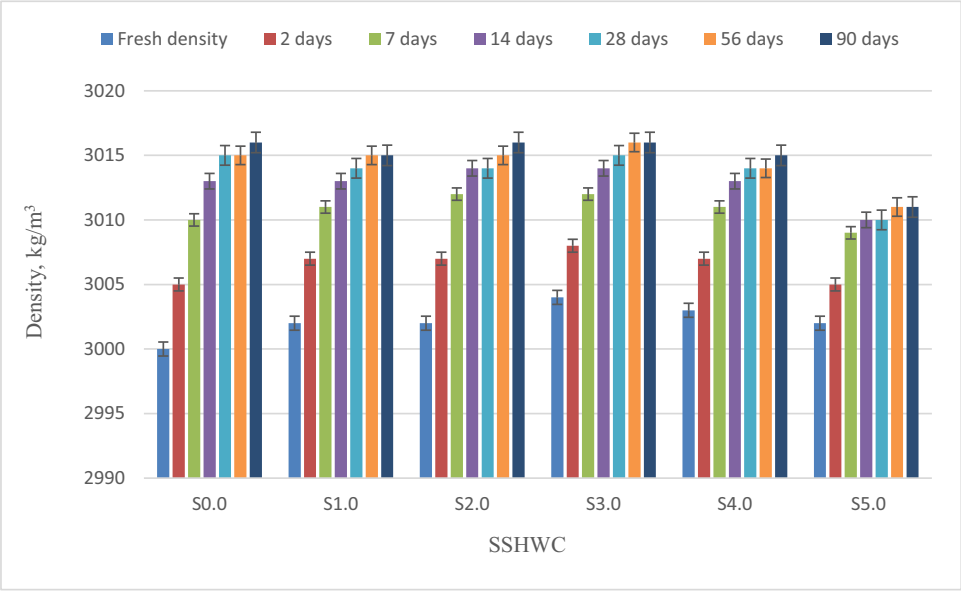

Figure 7: Fresh and hardened density of SSHWC.

properties were also affected negatively at higher NSS content (>4.0%). The radiation shielding property of hardened concretes is affected by the presence of voids.

The concrete containing 5.0% and 3.0% NSS by weight of cement content showed density values of 3,010 and 3,015 kg/m^3 respectively. The NSS content should be optimized to ensure an optimal concrete density and physicomechanical characteristics [65]. With the increasing curing period, the mass density of most mixes increased. In addition, the improvements were apparent until the 28th curing day. Under prolonged curing, the samples show a dense microstructure with continuous cement hydration [13]. The mixes S4.0 or S5.0 showed improved hardened density; however, higher amounts of NSS can inverse the effect of the micromorphology of the produced C–S–H gel [63].

4.4 Compressive strength

The CS reflects the quality of hardened concrete. The test result is a direct reflection of the quality of the concrete. It is believed that the physical and mechanical properties of the components of ASFS help in achieving high SSHWC packing density and strength performance. The low w/c ratios were attained because of the activity of the superplasticizer and the optimal cement content used. These factors are essential for SSHWC development for all mixtures, including the control mix [8].

Although the concretes generally showed good performances, the presence of NSS further improved their performance. Previously, the improved performance of concrete upon adding the nano-silica was believed because of the filler effect of the added nano-silica [66]. However, recent studies have shown that this improvement comes from the small size of the introduced nano-silica. It offered a large surface area that encouraged the rate of cement hydration and pozzolan reactions, which leads to an early higher strength [13]. According to the values in Figure 8, the CS of the SSHWC was directly at the 0.0–3.0% NSS content. Besides, there was a decline in the CS, as the NSS content (4.0–5.0%) exceeded the cement reaction limit [67].

As illustrated in Figure 8, the CS enhancement was evident at an early age compared to the control mix. The CS of concretes was improved by adding 3.0% NSS by cement weight. The CS of all hardened concrete increased until the 28th day of curing because of the increase in the cement paste efficacy during the primary cement hydration. However, there was a decline in the rate of CS development after 28 days; it was virtually nonexistent even when the curing period was extended [68].

The CS of the SSHWC mixes, namely S0.0, S1.0, S2.0, S3.0, S4.0, and S5.0, met the CS requirement of grade 100 HWC after 28 days of curing. Besides, the ideal SSHWC (S3.0) obtained the maximum CS value [8]. The small increase in CS with adding the NSS could make a significant difference in radiation isolation, which is the primary objective of this study [8].

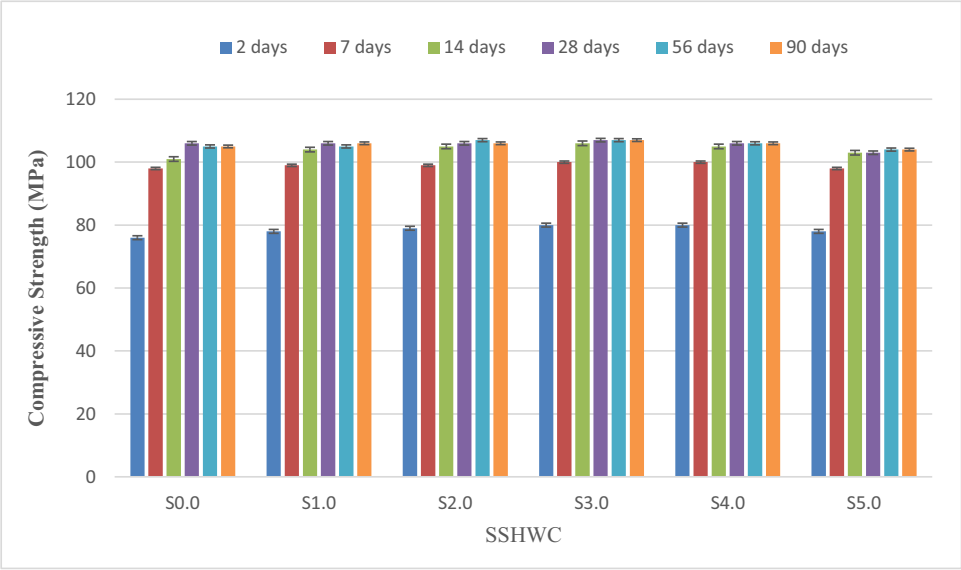

Figure 8: The SSHWC CS.

4.5 Ultrasonic pulse velocity

The ultrasonic pulse velocity test is one of the nondestructive tests for the quality assessment of SSHWC. During this test, the longitudinal ultrasonic waves are propagated through the length of the concrete material. The UPV test aims to record the velocity value of this wave, as it is propagated throughout the material [69]. The UPV values of SSHWC prepared with different NSS contents are shown in Figure 9. The observed UPV values followed the same trend of the CS outcome. The UPV values of SSHWC after 2 days of age were significantly lower than those of samples at 28 days of age. It could be because of the increasing rate of cement hydration with age, which comes with greater microstructural compaction [70].

The UPV values of the 28 days showed the role of NSS in increasing the density of mixes S2.0 and S3.0. It is evidenced by the UPV values of the mixes, which exceeded 5,000 m/s. The mix S5.0 exhibited lower UPV value because of its greater porous microstructure, as a result of the larger quantity of added NSS. At 56 and 90 days of age, there was no noticeable improvement in the UPV values of SSHWC, when matched to the values at 28 days of age. It could be because of primary cement hydration, which was near completion by the 28th day [71].

In general, at the age of 7 days, the mixes S1.0, S2.0, S3.0, S4.0, and S5.0 showed excellent UPV values of >4,650 m/s. However, the UPV performances were excellent (>4,850 m/s) at the age of 28 days for all mixes (S0.0, S1.0, S2.0, S3.0, S4.0, and S5.0). In an earlier study, the UPV values ranging from 4,300 to 4,650 ms^{-1} are considered good. The quality of the concrete is considered as excellent when its value exceeded 4,650 ms^{-1} [45]. All the concrete mixes used in the study were considered to exhibit excellent quality at the age of 28 days and beyond.

4.6 Split tensile strength

The split tensile strength (STS) of SSHWC at different ages is shown in Figure 10. Observably, there was a slight increase in the STS value with increases in the NSS content from 1.0% to 3.0% by weight of cement. The observed increase in the STS value of SSHWC indicates improved bond strength between aggregates and cement. Besides, a decline was observed in the STS value of mixes S4.0 and S5.0 from the optimum. It was because of the effect of high NSS amount, which negatively impacted the reaction of the cement and caused the development of voids and gaps in the mix [13].

The properties of ASFS contribute to a high STS performance [72] as its irregular shape is necessary for the production of concretes with good tensile strength [47]. However, the decline in the STS of S5.0 could be caused by the weakness of the ITZ between the aggregate and the paste matrix (Figure 10). On the contrary, the rest of the mixes performed well in terms of tensile strength with the inclusion of NSS. The trend may also be because of a stronger developed ITZ [67]. The STS behavior of SSHWC is similar to the CS of SSHWC and the UPV results [8].

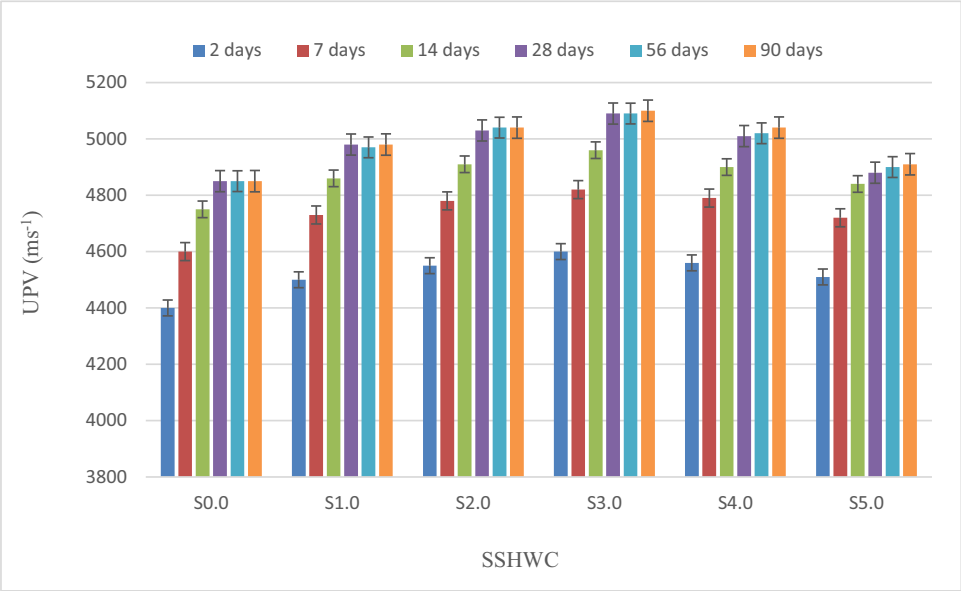

Figure 9: UPV of SSHWC mixes.

4.7 Water absorption

SSHWC mixes prepared with different NSS contents were evaluated for water absorption capability at different ages, as depicted in Figure 11. The samples showed improved water absorption capacity with age (from 2 to 28 days). However, it showed no discernible improvement in water absorption at older ages (28–90 days). It could be because of the high rate of cement hydration at an early age, and it was near to completion by 28 days [73,74]. The water absorption values of the mixes S3.0 and S4.0 were below 0.65% by the age of 7 days. At the same age, the control mix recorded 0.8% water absorption test value. These good results agreed with those of the mechanical tests. Besides, the water absorption test values could be caused by the irregular shape of the aggregate, as it interacted well with the superplasticizer to improve the structure of the paste-aggregate pore. The aggregates' mechanical properties also improved the durability of the concrete. Water

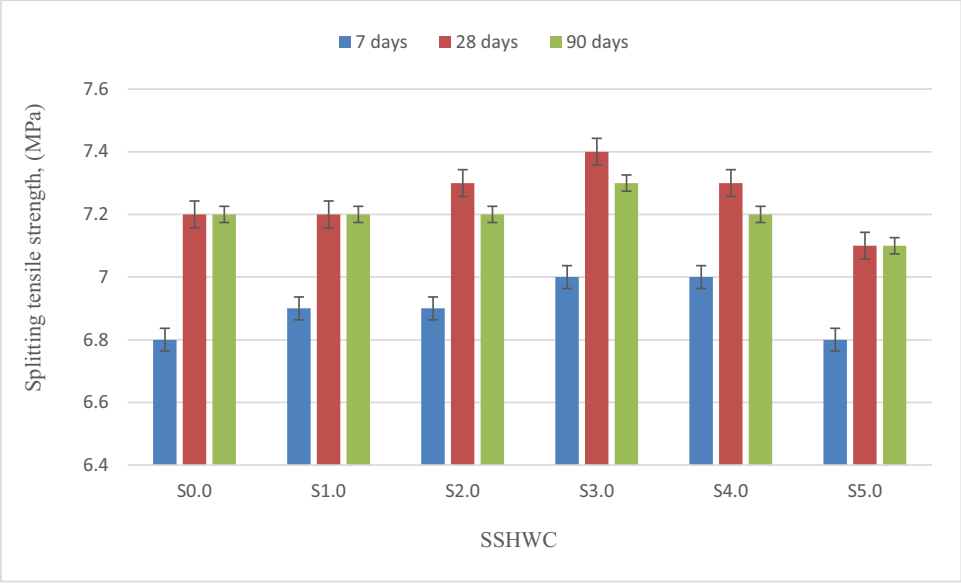

Figure 10: Splitting tensile strength of SSHWC mixes.

absorption was impeded by the impermeable voids present in the aggregates.

Concrete mixes S2.0, S3.0, and S4.0 showed significantly lower water absorption test value. This is because of the filler action of NSS which filled the voids (action physically) and accelerated primary cement hydration (action chemically) to form a dense network of C–S–H gel [75]. This observation is consistent with previous research. Zareei et al. [76] observed that the inclusion of nano-silica led to a 35% reduction in the water absorption of the concrete because of the micro-filling effect of nano-silica particles. The water absorption rate of the mix S5.0 mix was significantly higher than that of mix S3.0 because of internal voids and gaps that weakened the ITZ [71]. The pessimistic effect of NSS with 5% could be attributed to the extra water content of the stabilizer of the NSS. It adds more water to the total amount of the mixture of water content. The addition of nano-silica beyond the optimum limit has been reported to negatively affect the mechanical strength of the resulting concrete [77].

4.8 Capillary absorption

SSHWC mixes produced with different NSS contents were tested for capillary action. The results are presented in Figure 12. The reason for this test is to determine the relative volume of capillary pores present in the mixtures. This test also explains the resistivity of the concrete to the penetration of harmful ions, such as sulfate and chloride, through capillary actions. The deleterious ions will affect the long-term concrete durability upon penetration [71]. From the capillary test results, it was observed that within the first 8 h, the capillary absorption rate was higher, as the whole mixes achieved a steep linear gradient. It was because of the influx of water saturated of the large capillary voids in the matrix through capillary action. The control mix (S0.0) and mix S5.0 showed the maximum capillary absorption rate within the first 8 h.

Besides, the capillary absorption rate was lowest in S1.0, S2.0, S3.0, and S4.0 mixes. The results indicated that within the cement paste matrix, S0.0 and S5.0 had the maximum relative volume of the continuous capillary pores. Because of the high capillary absorption rate, the resistance of S0.0 and S5.0 to aggressive ion penetration would be lower than the other NSS mixes. It was because of the role of the NSS in improving the properties of the resulting concrete. The NSS content is not recommended to exceed the limits, which may affect the properties of the resulting concrete as in the case with mix S5.0 [78]. Throughout the test, the capillary absorption rates for mixes S1.0, S2.0, S3.0, and S4.0 were lower than mixes S0.0 and S5.0.

The capillary absorption of mix S3.0 was significantly improved compared to the control mix (S0.0). The effect was optimistic, with an increase of 5.2% in capillary values at 1 h and 1% after 28 days of testing [79,80]. These

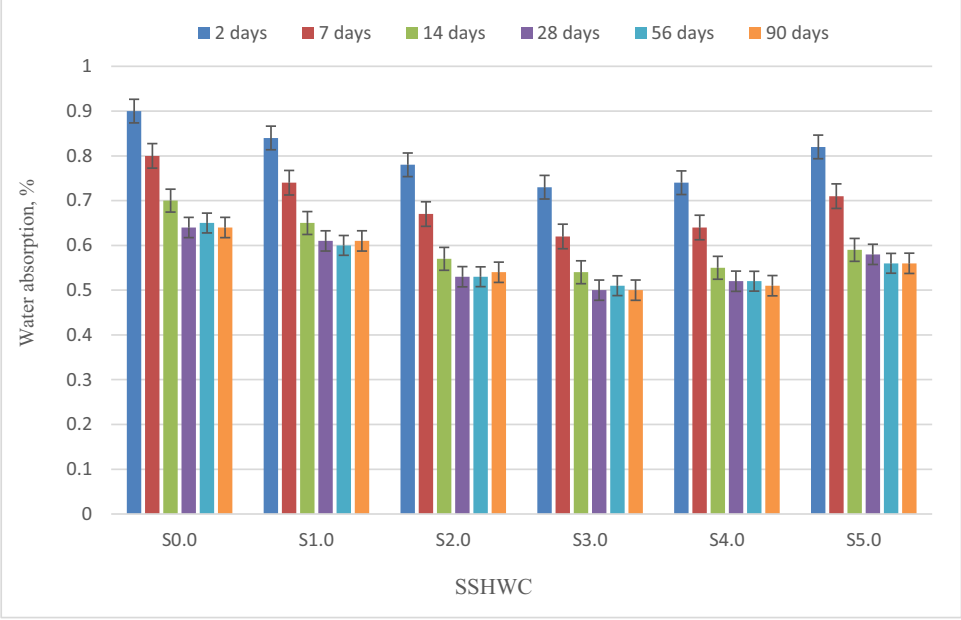

Figure 11: Water absorption of SSHWC mixes.

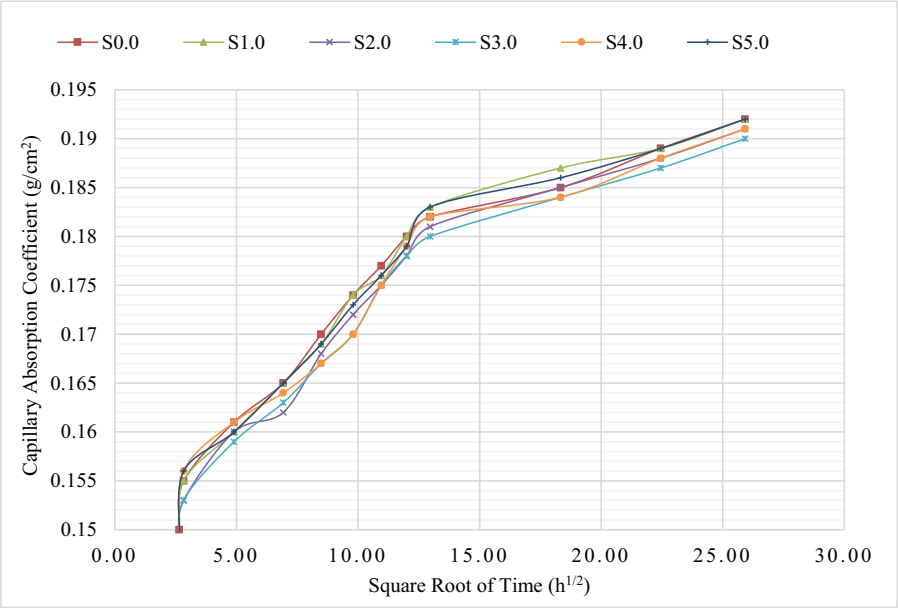

Figure 12: Capillary absorption of SSHWC mixes.

results agreed with previous studies that reported improvement in capillary absorption property upon addition of 1.5% and 3% of nano-silica and micro-silica, respectively [26]. These results also indicated the important role of NSS in C–S–H gel nucleation and capillary pores filling in the concrete. The irregular shape of the aggregates and the superplasticizer can also influence the capillary absorption of SSHWC, as the excellent cement paste–aggregates interaction will reduce the voids [71].

As the water absorption and capillary absorption tests reveal the fluid transport capabilities of concrete, they are considered the most two significant tests for HWC. Both tests also show the extent to which the concrete contains continuous and discontinuous pores and voids. In addition, the test results indicate the ability of the concrete to attenuate radiation in the same context [12]. Besides, the distribution of pore sizes showed narrowing of the large capillary pores by the nano-silica because of the combined effect of the nano-filler and the pozzolanic reaction [81]. The capillary absorption test presented similar results as the water absorption test. Both findings were in line with the trend of mechanical tests.

4.9 SEM analysis

One of the most important tests in HWC evaluation is the SEM test. This test provides a clear understanding of the concrete microstructure. The best way for spreading harmful radiation through concrete is the air void. Therefore, the serious consideration that was taken to ensure all voids is filled in the internal structure of the concrete. This is to make sure that the radiation attenuation property can be improved [8]. The reason for the SEM analysis of the microstructure of the concrete was to check the ITZ and binder phase performances. The analysis was carried out on the control mix (S0.0), the optimum concrete mix (S3.0), and mix with NSS 5.0%. The comparison between the SEM observations of these samples is shown in Figure 13. The framework of the C–S–H gel was also evaluated at 28 days of age. For this study, the backscatter SEM mode was used to ensure a clear observation of the internal microstructure of the samples. In Figure 13(a–c), the internal structure of S0.0, S3.0, and S5.0 is displayed at 500× magnification. The general sample morphology was examined at the magnification level of 500×. From the results of the SEM, the mix S3.0 showed a significantly denser internal microstructure compared to S0.0 and S5.0 mixtures. This is consistent with the observations of Zhang et al. [82] who reported that nano-SiO_2 particle improved the microscopic structure of cementitious composites. On the contrary, the more nanomaterials content as in mix S5.0 will effect inversely on the produced concrete microstructure [13,83].

In contrast, the microstructure of mixes S0.0 and S5.0 (Figure 13a and c) had microcracks in the ITZ and cement paste matrix. Although microcracks were also present in S3.0, as shown in Figure 13(b), the number

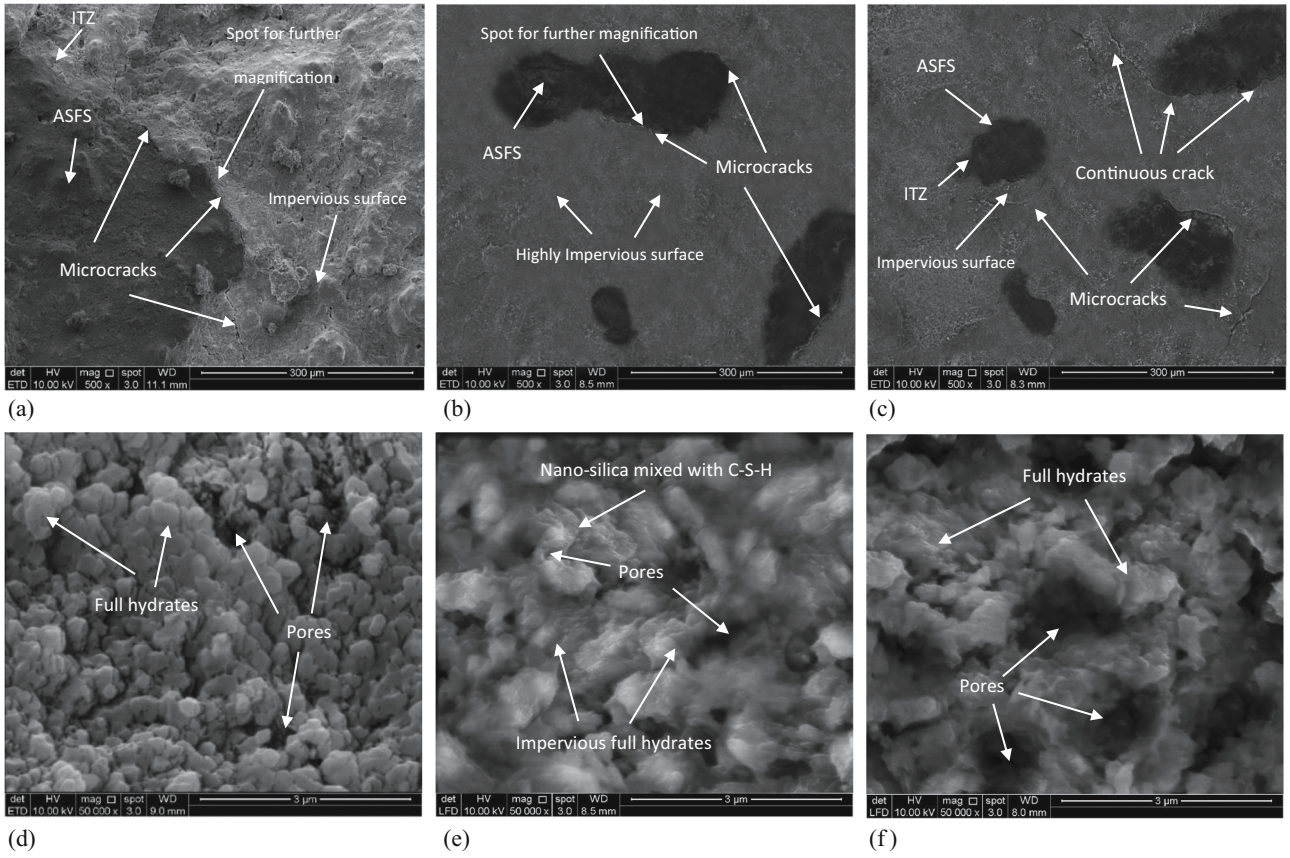

Figure 13: SEM images of SSHWC at 28 days curing age. (a) S0.0 SSHWC at 500× [13]. (b) S3.0 SSHWC at 500×. (c) S5.0 SSHWC at 500×. (d) S0.0 SSHWC at 50,000× [13]. (e) S3.0 SSHWC at 50,000×. (f) S5.0 SSHWC at 50,000×.

and width of cracks were significantly less than S0.0 and S5.0. Consequently, the NSS particles are considered useful in improving binder phase microstructural density for the content used in S3.0 [84]. Furthermore, the SEM evaluation was carried out at higher magnifications (10,000× and 50,000×) to have a more unobstructed view for the sample micromorphology at the binder phase. As evidenced in Figure 13(d–f), the micrographs of S0.0, S3.0, and S5.0 showed a complete cement paste reaction at 50,000× magnification, as it has formed a well-defined C–S–H framework [8]. Despite the good performance of mix S0.0 in developing the C–S–H gel, there were visible micropores, as shown in Figure 13(d).

Regarding the mix S3.0, as shown in Figure 13(e), it showed a uniform and impervious C–S–H gel network with few micropores when compared to S0.0. It explains the efficiency of an optimum NSS content in improving the rate of cement reaction, which leads to the development of additional C–S–H gel and forming an impervious C–S–H gel network. Even though the NSS at 3.0% filled the remaining nano-voids, it did not affect the cement reaction [84]. Besides, the increase in NSS up to 5.0% shows a pessimistic result as shown in Figure 13(f), and this agrees with the results obtained by Khalaf et al. [13]. It could be because of the inadequate space required to form hydration products. Besides, the excessive amount of nanoparticles would also lead to uniform dispersion difficulties.

Based on the SEM micrographs (Figure 13g–i), the magnitude of the crack width in S0.0 and S5.0 was found to be significantly larger when compared to the mix S3.0. The smaller size of the crack in S3.0 could be because of additional C–S–H gel formation, which led to a denser paste matrix when compared to the other mixtures [84]. The SEM observation confirmed a denser matrix of the S3.0 mix that resulted in better mechanical performance and resistance to the transport of fluids compared to S0.0 and S5.0.

The outcome of this test agrees with the results of the study by Li [85]. It indicated that the nano-silica would strengthen the concrete microstructure and help in filling in the blanks. The amount of calcium hydroxide crystals is formed because of the hydration reaction between cement and water. The $Ca(OH)_2$ crystal is hexagonal; it

facilitates the binding of the aggregates with the paste matrix in the ITZ so that it affects the concrete's performance. The nano-silica has a high specific surface area as compared with micro-silica; it shows high activity. It can react quickly with $Ca(OH)_2$ to form C–S–H gels; the outcome of this reaction is reducing the crystal size and the quantity of $Ca(OH)_2$. As the C–S–H gel occupies the voids, the ITZ increases in density, thereby increasing the volume of the binding paste matrix. The C–S–H gel is composed of 70% of the hydration products; its relative diameter is around 10 nm. The filling of the voids in the structure of C–S–H gel by nano-silica particles increases the paste matrix density. The nano-silica particles can act as a nucleus in the structure of C–S–H gel, which facilitate the formation of a strong bond with the C–S–H gel particles. It improves the reliability of the hydration product structure. In addition, it improves the long-term mechanical properties of the concrete.

5 X-ray radiation shielding

The X-ray analysis presents one of the most significant findings of the study. The test accomplishes the prime purpose of producing the type of concrete that is suitable for the X-ray shielding application. The main idea of adding NSS is to improve the shielding ability of the concrete to X-rays. An overview of this work or its main concept is given in Figure 14. The μ, HVL, and TVL of the SSHWC mixes are presented in Table 3. The increase in the Z_{eff} of the material with NSS addition improved the ability of the concrete to isolate X-rays. The reason is that NSS particles have adequately covered the cement particles, as demonstrated by the zeta potential test. On the contrary, the NSS significantly contributes to improving the X-rays shielding property of the concrete by filling the fine voids with the cement paste and the ITZ, as proven by the SEM and durability tests. The optimum mix composition with superior radiation insulation property among all mixes is mix S3.0. By comparing the mix with the reference mix S0.0, it was found that the difference between them was only the percentage of NSS addition by cement weight. At a small NSS addition level, the radiation isolation property was improved by 6.4% because of the effectiveness of the NSS in enhancing all the studied properties. The result agreed with the observation of [86] regarding the improvement of the concrete properties to isolate harmful X-rays by adding fine glass powder.

A relative improvement was found in the ability of SSHWC X-ray isolation between 7 and 28 days, as shown in Figure 15. It was mainly because of the increase in material density along with an increase in C–S–H gel formation during a prolonged curing duration of up to 28 days [87]. With a longer curing duration of up to 90 days, there was no significant change in X-ray radiation isolation property. The results are consistent with the mechanical and durability test results. The logical reason for this is the completion of early-age cement reaction. In other words, there is no noticeable increase in the density of concrete after the age of 28 days [88]. The TVL and HVL values are the thickness of the concrete material which is required to reduce the intensity of radiation to 10% and 50% of the initial intensity, respectively. The HVL and TVL are often inversely proportional to the μ as mentioned in Table 3. The thickness can be reduced by about

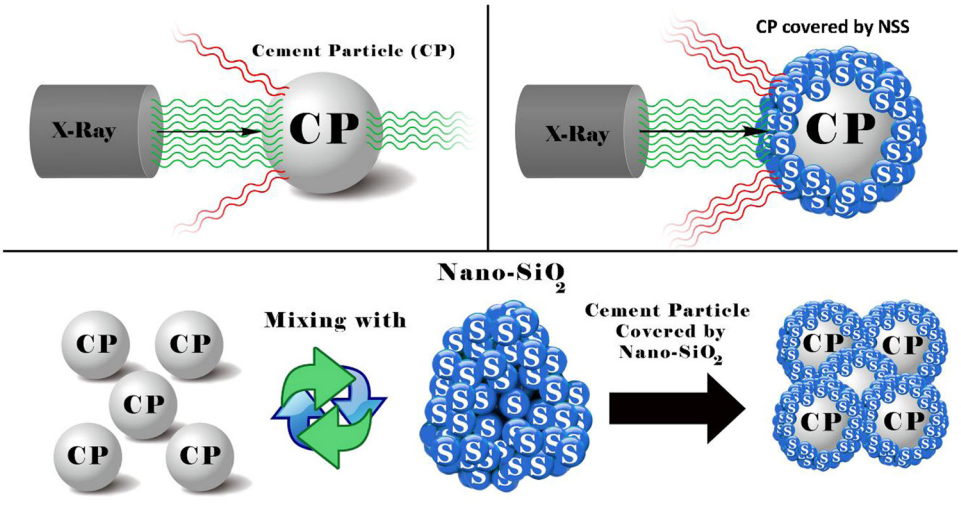

Figure 14: The role of NSS in enhancing the shielding capability of the produced SSHWC.

Table 3: Relationship between HVL, TVL, and μ of SSHWC mixes subjected to X-Ray

Mixes	μ (cm^{-1})			HVL (cm)			TVL (cm)		
	7 days	28 days	90 days	7 days	28 days	90 days	7 days	28 days	90 days
S0.0	0.0833	0.0858	0.0860	8.32	8.07	8.05	27.64	26.83	26.77
S1.0	0.0854	0.0874	0.0876	8.11	7.93	7.91	26.96	26.34	26.28
S2.0	0.0870	0.0893	0.0890	7.96	7.76	7.78	26.46	25.78	25.87
S3.0	0.0888	0.0913	0.0914	7.8	7.59	7.58	25.93	25.21	25.19
S4.0	0.0877	0.0899	0.0896	7.9	7.71	7.73	26.25	25.61	25.69
S5.0	0.0864	0.0881	0.0878	8.02	7.86	7.89	26.65	26.13	26.22

6.4% when SSHWC is produced by 3% NSS by weight of cement. It shows the effectiveness of the NSS in improving the X-ray insulation of SSHWC. Thus, the incorporation of NSS into HWC enhanced all the mechanical, microstructural, durability, and radiation insulation properties in the work.

6 γ-Ray radiation shielding

The photon energy of 59.54 keV from the Am 241 radioactive source was used to determine the HVL, TVL, and μ of the samples. The results of the tests are presented in Table 4, whereas Figure 16 presents the differences in the values of μ at different radiation protective potentials of the concretes at 7, 28, and 90 days of age. These values were measured based on the γ-ray emitted from the Am 241 source. Observably, there were increases in the values of μ as the sample density increases [8]. This is because of the presence of more electrons in dense materials, which promote further interactions. As a result, the photon energy is reduced. However, the test results indicated that the addition of NSS had a marginal effect on the radiation isolation of the γ-ray. The finding was distinct as compared to the observation of X-ray attenuation. It was because of the difference between the γ-ray and X-ray, even though both are types of electromagnetic radiation. Gamma-rays are nuclear particles (produced by the decay of nuclei), whereas X-rays are extra-nuclear. The gamma-rays have a higher frequency, and therefore, it is more energetic and penetrative compared to the X-ray photons [89].

The comparison of mix S3.0 (optimum mix) and mix S0.0 (control mix) showed only a small difference in the material composition upon addition of 3% NSS. The resulting concrete also showed improvement in density and performance, as the presence of NSS at 3% encouraged the development of more C–S–H gel [13]. The NSS should be used below the content of 4.0% to achieve concrete with better γ-ray attenuation property, according to the results presented in Table 4. As the NSS is in excessive amounts, it would affect the interaction with cement,

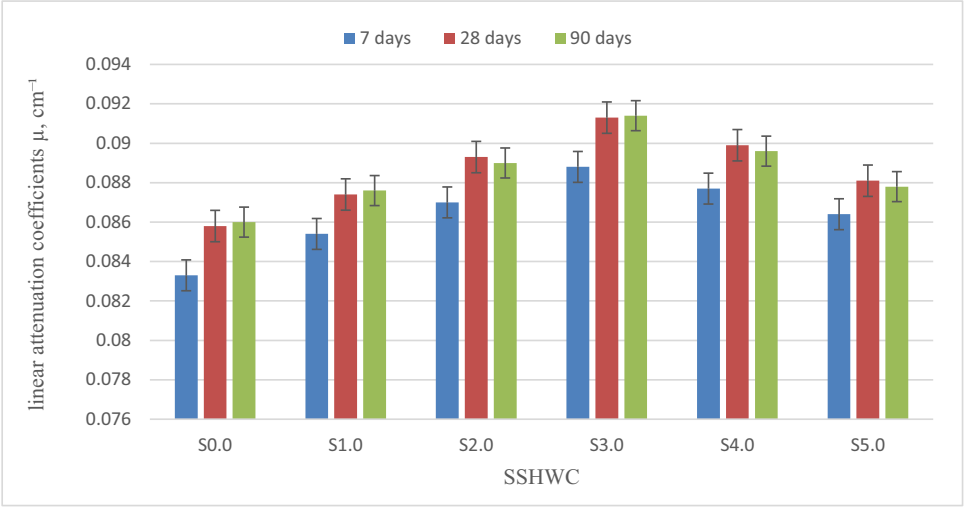

Figure 15: Linear attenuation coefficient (μ) at 7, 28, and 90 days for concrete with different NSS contents.

Table 4: Relationship between HVL, TVL, and μ of SSHWC mixes subjected to γ-Ray

Mixes	μ (cm^{-1})			HVL (cm)			TVL (cm)		
	7 days	28 days	90 days	7 days	28 days	90 days	7 days	28 days	90 days
S0.0	0.2901	0.3001	0.3009	2.39	2.31	2.30	7.93	7.67	7.65
S1.0	0.2961	0.3004	0.3006	2.34	2.30	2.30	7.77	7.66	7.65
S2.0	0.2977	0.3007	0.3007	2.32	2.30	2.30	7.73	7.65	7.65
S3.0	0.2989	0.3012	0.3013	2.32	2.30	2.30	7.70	7.64	6.64
S4.0	0.2985	0.3008	0.3008	2.32	2.30	2.30	7.71	7.65	7.65
S5.0	0.298	0.3003	0.3004	2.32	2.30	2.30	7.72	7.66	7.66

Figure 16: Linear attenuation coefficient (μ) of different SSHWC mixes at different ages.

thereby creating more internal voids as a result of weak bonding [69]. The TVL and HVL values are normally used to determine the attenuation properties of most absorbers [13].

In this study, the TVL and HVL of the emitted γ-rays from the Am 241 source for all the studied mixes are tabulated in Table 4. The table showed a gradual decline in the TVL and HVL values of the mixes as their densities are increasing. Low HVL and TVL values normally indicate good radiation shielding properties of the materials [90]. The TVL and HVL values of S3.0 were slightly lower than S0.0, possibly because of the higher density of S3.0 compared to that of S0.0. Ameri et al. [91] stated that incorporating CS in concrete mixes increased the density, and as a result, the attenuation thickness was reduced. These observations give a clear indication of the indirect relationship between HVL/TVL values and sample density [92]. It also evidenced that the γ-ray attenuation capacity of SSHWC can be improved with NSS if used at the appropriate addition level.

7 Conclusion

The SSHWC containing NSS, which contains the ASFS, shows high engineering performance and better radiation shielding properties. The use of NSS at 3% by weight of cement improved the physical, mechanical, and radiation shielding properties of the studied concrete. It is not recommended to use the NSS as a concrete additive in the HWC at more than 4% content by cement weight, as it will have an adverse effect on the cement reaction. The radiation attenuation property of HWC produced with ASFS against X-ray was improved by up to 6.4% upon the addition of NSS as a concrete additive.

Acknowledgments: The financial support for this study was provided by the Ministry of Science, Technology and Innovation (MOSTI) of Malaysia through the International Collaboration Fund (ICF) (Reference. No. IF0420I1224) with the project title “The optimization of mineral processing of coal bottom ash for large volume reuse as

constituent binder and aggregate for concrete production at industrial scale". Other form of implicit and explicit support from Universiti Sains Malaysia in the course of carrying out the work which led to the publishing of this work is duly acknowledged.

Conflict of interest: The authors declare no conflict of interest regarding the publication of this paper.

References

[1] Nadeem M, Pofale AD. Experimental investigation of using slag as an alternative to normal aggregates (coarse and fine) in concrete. Int Struct Eng. 2012;3(1):117–27.
[2] Reiterman P, Holčapek O, Zobal O, Keppert M. Freeze–thaw resistance of cement screed with various supplementary cementitious materials. Rev Adv Mater Sci. 2019;58(1):66–74.
[3] Sosa I, Thomas C, Polanco JA, Setién J, Tamayo P. High performance self-compacting concrete with electric arc furnace slag aggregate and cupola slag powder. Appl Sci. 2020;10(3):773.
[4] Ameri F, Shoaei P, Musaeei HR, Zareei SA, Cheah CB. Partial replacement of copper slag with treated crumb rubber aggregates in alkali-activated slag mortar. Constr Build Mater. 2020;256:119468.
[5] Shoaei P, Ameri F, Musaeei HR, Ghasemi T, Cheah CB. Glass powder as a partial precursor in Portland cement and alkali-activated slag mortar: A comprehensive comparative study. Constr Build Mater. 2020;251:118991.
[6] Zamanabadi SN, Zareei SA, Shoaei P, Ameri F. Ambient-cured alkali-activated slag paste incorporating micro-silica as repair material: Effects of alkali activator solution on physical and mechanical properties. Constr Build Mater. 2019;229:116911.
[7] Yüksel İ. A review of steel slag usage in construction industry for sustainable development. Env Dev Sustai. 2017;19(2):369–84.
[8] Khalaf MA, Ban CC, Ramli M, Ahmed NM, Sern LJ, Khaleel HA. Physicomechanical and gamma-ray shielding properties of high-strength heavyweight concrete containing steel furnace slag aggregate. J Build Eng. 2020;30:101306.
[9] Ikraiam F, El-Latif AA, ELazziz AA, Ali J. Effect of steel fiber addition on mechanical properties and γ-ray attenuation for ordinary concrete used in El-Gabal El-Akhdar area in Libya for radiation shielding purposes. Arab J Nucl Sci Appl. 2009;42:287–95.
[10] Abdo AE-S. Calculation of the cross-sections for fast neutrons and gamma-rays in concrete shields. Ann Nucl Energy. 2002;29(16):1977–88.
[11] Akkurt I, Başyigit C, Akkaş A, Kilingarslan Ş, Mavi B, Giinoglu K. Determination of some heavyweight aggregate half value layer thickness used for radiation shielding. Acta Phys Pol A. 2012;121(1):138.
[12] Khalaf MA, Ban CC, Ramli M. The constituents, properties and application of heavyweight concrete: A review. Constr Build Mater. 2019;215:73–89.
[13] Khalaf MA, Cheah CB, Ramli M, Ahmed NM, Al-Asady AMA, Ali AMA, et al. Engineering and gamma-ray attenuation properties of steel furnace slag heavyweight concrete with nano calcium carbonate and silica. Constr Build Mater. 2020;120878.
[14] Li Z, Sheng P, Siu W-L. Low-frequency soundproof concrete. Mag Concr Res. 2003;55(2):177–81.
[15] Oto B, Gür A. Gamma-ray shielding of concretes including magnetite in different rate. Int J Phys Sci. 2013;8(8):310–4.
[16] Demir F, Budak G, Sahin R, Karabulut A, Oltulu M, Un A. Determination of radiation attenuation coefficients of heavyweight-and normal-weight concretes containing colemanite and barite for 0.663 MeV γ-rays. Ann Nucl Ener. 2011;38(6):1274–8.
[17] Ling T-C, Poon C-S, Lam W-S, Chan T-P, Fung KK-L. X-ray radiation shielding properties of cement mortars prepared with different types of aggregates. Mater Struct. 2013;46(7):1133–41.
[18] Mohammadi H, Bahrololoumi A, Chen Y, Dargazany R. A micromechanical model for constitutive behavior of elastomers during thermo-oxidative aging. Constitutive Models for Rubber XI. Boca Raton, Florida, United States: CRC Press; 2019. p. 542–7.
[19] Pacheco-Torgal F, Miraldo S, Ding Y, Labrincha J. Targeting HPC with the help of nanoparticles: An overview. Constr Build Mater. 2013;38:365–70.
[20] Chu Y-S, Davaabal B, Kim D-S, Seo S-K, Kim Y, Ruescher C, et al. Reactivity of fly ashes milled in different milling devices. Rev Adv Mater Sci. 2019;58(1):179–88.
[21] Bhaskar S, Kumar M, Patnaik A. Mechanical and Tribological overview of ceramic particulates reinforced aluminium alloy composites. Rev Adv Mater Sci. 2019;58(1):280–94.
[22] Ossai CI, Raghavan N. Nanostructure and nanomaterial characterization, growth mechanisms, and applications. Nanotechnol Rev. 2018;7(2):209–31.
[23] Kawashima S, Hou P, Corr DJ, Shah SP. Modification of cement-based materials with nanoparticles. Cem Concr Compos. 2013;36:8–15.
[24] Guo K, Miao H, Liu L, Zhou J, Liu M. Effect of graphene oxide on chloride penetration resistance of recycled concrete. Nanotechnol Rev. 2019;8(1):681–9.
[25] Singh L, Karade S, Bhattacharyya S, Yousuf M, Ahalawat S. Beneficial role of nanosilica in cement based materials–A review. Constr Build Mater. 2013;47:1069–77.
[26] Nili M, Ehsani A, Shabani K. Influence of nano-SiO_2 and microsilica on concrete performance. Sec Int Con. 2010;1–5.
[27] Zhao Z, Qi T, Zhou W, Hui D, Xiao C, Qi J, et al. A review on the properties, reinforcing effects, and commercialization of nanomaterials for cement-based materials. Nanotechnol Rev. 2020;9(1):303–22.
[28] Ismaeel NS, Khalaf MA. Properties of high strength concrete containing stonepowder as natural pozzolanic materials. J Univ Anbar Pure Sci. 2013;7(2):77–84.
[29] Ismaeel NS. Properties of high performance concrete containing stone powder as replacement of cement. Tik J Eng Sci. 2013;20(4):49–54.
[30] Lin Q, Chen Y, Liu C. Mechanical properties of circular nanosilica concrete filled stainless steel tube stub columns after being exposed to freezing and thawing. Nanotechnol Rev. 2019;8(1):600–18.

[31] Campillo I, Dolado J, Porro A. High-performance nanostructured materials for construction. Spec Publ R Soc Chem. 2004;292:215–26.
[32] Said AM, Zeidan MS, Bassuoni M, Tian Y. Properties of concrete incorporating nano-silica. Constr Build Mater. 2012;36:838–44.
[33] Hou P, Qian J, Cheng X, Shah SP. Effects of the pozzolanic reactivity of nanoSiO_2 on cement-based materials. Constr Build Mater. 2015;55:250–8.
[34] Land G, Stephan D. Controlling cement hydration with nanoparticles. Cem Concr Compos. 2015;57:64–7.
[35] Kontoleontos F, Tsakiridis P, Marinos A, Kaloidas V, Katsioti M. Influence of colloidal nanosilica on ultrafine cement hydration: Physicochemical and microstructural characterization. Constr Build Mater. 2012;35:347–60.
[36] Oltulu M, Şahin R. Pore structure analysis of hardened cement mortars containing silica fume and different nano-powders. Constr Build Mater. 2014;53:658–64.
[37] Gesoglu M, Güneyisi E, Asaad DS, Muhyaddin GF. Properties of low binder ultra-high performance cementitious composites: Comparison of nanosilica and microsilica. Constr Build Mater. 2016;102:706–13.
[38] Sanchez F, Sobolev K. Nanotechnology in concrete – A review. Constr Build Mater. 2010;24(11):2060–71.
[39] Amin M, Abu, el-Hassan K. Effect of using different types of nano materials on mechanical properties of high strength concrete. Constr Build Mater. 2015;80:116–24.
[40] He K, Chen Y, Xie W. Test on axial compression performance of nano-silica concrete-filled angle steel reinforced GFRP tubular column. Nanotechnol Rev. 2019;8(1):523–38.
[41] Ghafari E, Costa H, Júlio E, Portugal A, Durães L. The effect of nanosilica addition on flowability, strength and transport properties of ultra high performance concrete. Mater Des. 2014;59:1–9.
[42] Jo B-W, Kim C-H, Tae G-h, Park J-B. Characteristics of cement mortar with nano-SiO_2 particles. Constr Build Mater. 2007;21(6):1351–5.
[43] Rong Z, Sun W, Xiao H, Jiang G. Effects of nano-SiO_2 particles on the mechanical and microstructural properties of ultra-high performance cementitious composites. Cem Concr Compos. 2015;56:25–31.
[44] Khalaf MA, Ban CC, Ramli M. The constituents, properties and application of heavyweight concrete: A review. Constr Build Mater. 2019;215:73–89.
[45] Nikbin IM, Mohebbi R, Dezhampanah S, Mehdipour S, Mohammadi R, Nejat T. Gamma ray shielding properties of heavy-weight concrete containing nano-TiO_2. Radiat Phys Chem. 2019;162:157–67.
[46] Khitab A, Ahmad S, Munir M, Kazmi S, Arshad T, Khushnood R. Synthesis and applications of nano titania particles: A review. Rev Adv Mater Sci. 2018;53(1):90–105.
[47] Tobbala D. Effect of Nano-ferrite addition on mechanical properties and gamma ray attenuation coefficient of steel fiber reinforced heavy weight concrete. Constr Build Mater. 2019;207:48–58.
[48] British Standards Institution. BS EN 197-1 cement – Part 1: Composition, specifications and conformity criteria for common cements; 2007.
[49] American Society of Testing Materials. ASTM C494/C494M-13, standard specification for chemical admixtures for concrete. West Conshohocken, PA, USA: ASTM International; 2013.
[50] Physical and shielding protection parameterization of PbO-ZnO-B_2O_3-SiO_2 glass network. In: Razali NAN, Mustafa IS, Azman NZN, Kamari HM, Hashim ISM, Ahmad N, et al., editors. J Phys Conf Ser. Bristol, United Kingdom: IOP Publishing; 2018.
[51] Gencel O, Koksal F, Ozel C, Brostow W. Combined effects of fly ash and waste ferrochromium on properties of concrete. Constr Build Mater. 2012;29:633–40.
[52] Bahrololoumi A, Dargazany R. Hydrolytic aging in rubber-like materials: A micro-mechanical approach to modeling. IMECE. 2019;59469:V009T11A29.
[53] British Standards Institution. BS EN 26-1-2 Testing of concrete- Part 1: Fresh concrete- Section 2: Slump test; 2009a.
[54] British Standards Institution. BS EN 206 Concrete: Specification, performance, production and conformity; 2016.
[55] British Standards Institution. BS EN 12390-7:2009 Testing hardened concrete. Density of hardened concrete, London; 2009c.
[56] British Standards Institution. BS EN 12390-3 Testing hardened concrete, compressive strength of test specimens; 2009.
[57] British Standards Institution. BS EN12504-4 Testing of concrete- Part 4: Determination of ultrasonic pulse velocity; 2013.
[58] American Society of Testing Materials. ASTM C496-96 Standard test method for splitting tensile strength of cylindrical concrete specimens, annual book ASTM standards; 2011.
[59] British Standards Institution. BS EN 1881-122 Testing concrete- Part 122: Method for determination of water absorption; 1983.
[60] Benachour Y, Davy CA, Skoczylas F, Houari H. Effect of a high calcite filler addition upon microstructural, mechanical, shrinkage and transport properties of a mortar. Cem Concr Res. 2008;38(6):727–36.
[61] Tobbala D. Effect of Nano-ferrite addition on mechanical properties and gamma ray attenuation coefficient of steel fiber reinforced heavy weight concrete. Constr Build Mater. 2019;207:48–58.
[62] Rabeea MA, Owaid MN, Aziz AA, Jameel MS, Dheyab MA. Mycosynthesis of gold nanoparticles using the extract of flammulina velutipes, physalacriaceae, and their efficacy for decolorization of methylene blue. J Env Chem Eng. 2020;8(3):103841.
[63] Li W, Huang Z, Cao F, Sun Z, Shah SP. Effects of nano-silica and nano-limestone on flowability and mechanical properties of ultra-high-performance concrete matrix. Constr Build Mater. 2015;95:366–74.
[64] Ban CC, Kang CW, Wei OC. The influence of type and combination of polycarboxylate ether superplasticizer on the mechanical properties and microstructure of slag-silica fume ternary blended self-consolidating concrete. J Build Eng. 2020;31:101412.
[65] Tawfik TA, Metwally KA, El-Beshlawy S, Al Saffar DM, Tayeh BA, Hassan HS. Exploitation of the nanowaste ceramic incorporated with nano silica to improve concrete properties. J King Saud Univ Eng Sci. 2020.
[66] Kang CW, Ban CC, Wei OC, Ken PW, Heng LK. The properties of slag-silica fume ternary blended mortar with quarry dust. J Mech Eng Sci. 2020;14(1):6443–51.
[67] Mohammed B, Khed V, Nuruddin M. A review on nano-silica based concrete. J Nanomed Nanosci JNAN-128. 2017;2(5):1–4.
[68] Lim JS, Cheah CB, Ramli MB. The setting behavior, mechanical properties and drying shrinkage of ternary blended concrete

containing granite quarry dust and processed steel slag aggregate. Constr Build Mater. 2019;215:447–61.
[69] Hamidian M, Shariati M, Arabnejad M, Sinaei H. Assessment of high strength and light weight aggregate concrete properties using ultrasonic pulse velocity technique. Int J Phys Sci. 2011;6(22):5261–6.
[70] Cheah CB, Ramli M. The engineering properties of high performance concrete with HCWA–DSF supplementary binder. Constr Build Mater. 2013;40:93–103.
[71] Cheah CB, Lim JS, Ramli MB. The mechanical strength and durability properties of ternary blended cementitious composites containing granite quarry dust (GQD) as natural sand replacement. Constr Build Mater. 2019;197:291–306.
[72] Florez R, Colorado HA, Giraldo CH, Alajo A. Preparation and characterization of Portland cement pastes with Sm_2O_3 microparticle additions for neutron shielding applications. Constr Build Mater. 2018;191:498–506.
[73] Salih RM. Effect of water absorption on some mechanical and physical properties of epoxy/polyurethane blend reinforced with nano silica powder. Ira J Phy. 2017;15(32):92–8.
[74] Cheah CB, Ramli M. The fluid transport properties of HCWA–DSF hybrid supplementary binder mortar. Compos B Eng. 2014;56:681–90.
[75] Cheah CB, Lim JS, Ramli MB. The mechanical strength and durability properties of ternary blended cementitious composites containing granite quarry dust (GQD) as natural sand replacement. Constr Build Mater. 2019;197:291–306.
[76] Zareei SA, Ameri F, Bahrami N, Shoaei P, Moosaei HR, Salemi N. Performance of sustainable high strength concrete with basic oxygen steel-making (BOS) slag and nano-silica. J Build Eng. 2019;25:100791.
[77] Sbia LA, Peyvandi A, Soroushian P, Balachandra AM, Sobolev K. Evaluation of modified-graphite nanomaterials in concrete nanocomposite based on packing density principles. Constr Build Mater. 2015;76:413–22.
[78] Janković K, Stanković S, Bojović D, Stojanović M, Antić L. The influence of nano-silica and barite aggregate on properties of ultra high performance concrete. Constr Build Mater. 2016;126:147–56.
[79] Oltulu M, Şahin R. Effect of nano-SiO_2, nano-Al_2O_3 and nano-Fe_2O_3 powders on compressive strengths and capillary water absorption of cement mortar containing fly ash: A comparative study. Energy Build. 2013;58:292–301.
[80] Ban CC, Sern LJ, Jasme N. The mechanical strength and drying shrinkage behavior of high performance concrete with blended mineral admixture. J Teknol. 2019;81:4.
[81] Du H, Du S, Liu X. Durability performances of concrete with nano-silica. Constr Build Mater. 2014;73:705–12.
[82] Zhang P, Li Q-f, Wang J, Shi Y, Ling Y-f. Effect of PVA fiber on durability of cementitious composite containing nano-SiO_2. Nanotechnol Rev. 2019;8(1):116–27.
[83] Khongpermgoson P, Boonlao K, Ananthanet N, Thitithananon T, Jaturapitakkul C, Tangchirapat W, et al. The mechanical properties and heat development behavior of high strength concrete containing high fineness coal bottom ash as a pozzolanic binder. Constr Build Mater. 2020;253:119239.
[84] Li L, Huang Z, Zhu J, Kwan A, Chen H. Synergistic effects of micro-silica and nano-silica on strength and microstructure of mortar. Constr Build Mater. 2017;140:229–38.
[85] Ji T. Preliminary study on the water permeability and microstructure of concrete incorporating nano-SiO_2. Cem Concr Res. 2005;35(10):1943–7.
[86] Ling T-C, Poon C-S. A comparative study on the feasible use of recycled beverage and CRT funnel glass as fine aggregate in cement mortar. J Clean Prod. 2012;29:46–52.
[87] Ling T-C, Poon C-S, Lam W-S, Chan T-P, Fung KK-L. X-ray radiation shielding properties of cement mortars prepared with different types of aggregates. Mater Struc. 2013;46(7):1133–41.
[88] Preliminary study on influence of silica fume on mechanical properties of no-cement mortars. In: Cheah C, Nurshafarina J, editors. IOP Conf Ser Mater Sci Eng. Bristol, United Kingdom: IOP Publishing; 2019.
[89] Marelli M, Mignani R, De Luca A, Parkinson PS, Salvetti D, Den Hartog P, et al. Radio-quiet and radio-loud pulsars: Similar in gamma-rays but different in X-rays. Astrophys J. 2015;802(2):78.
[90] Fugaru V, Bercea S, Postolache C, Manea S, Moanta A, Petre I, et al. Gamma ray shielding properties of some concrete materials. Acta Phys Polonica A. 2015;127(4):1427–9.
[91] Ameri F, de Brito J, Madhkhan M, Taheri RA. Steel fibre-reinforced high-strength concrete incorporating copper slag: Mechanical, gamma-ray shielding, impact resistance, and microstructural characteristics. J Build Eng. 2020;29:101118.
[92] Azreen N, Rashid RS, Haniza M, Voo Y, Amran YM. Radiation shielding of ultra-high-performance concrete with silica sand, amang and lead glass. Constr Build Mater. 2018;172:370–7.